# Cavitation aggressiveness on a hydrofoil

Jean-Bastien Carrat, Timo Bouvard, Regiane Fortes Patella, Jean-Pierre Franc

# Cavitation aggressiveness on a hydrofoil

**JB Carrat, T Bouvard, R Fortes-Patella, JP Franc**

Univ. Grenoble Alpes, CNRS, Grenoble INP, LEGI, 38000 Grenoble, France

E-mail : regiane.fortes@legi.grenoble-inp.fr

**Abstract**. To improve the analyses of the cavitation erosion phenomena, cavitating flows around an instrumented hydrofoil were studied experimentally and numerically. The experiments allowed the assessment of cavitation aggressiveness by measurements from PVDF pressure sensors. A matrix of 8 PVDF sensors was built, installed and tested for several hydrodynamic conditions corresponding to different flow velocities, angles of attack and cavitation numbers. The unsteady cavitating flows were simulated by applying the in-house 2D code, referred to as "IZ". Unsteady Reynolds Averaged Navier-Stokes equations were solved for a homogeneous fluid with variable density. To model the cavitation phenomenon and to close the governing equation system, a barotropic state law was used associated with a modified k-ε RNG turbulence model. In order to evaluate the cavitation aggressiveness, simulations were coupled with a cavitation erosion model based on the energy balance between the cavitating flow, the vapour bubble collapses, the emitted pressure waves, and the neighbouring solid walls. The paper presents the experimental and numerical tools, the post-processing methodologies and the obtained results. A method was proposed to assess locally the cavitation aggressiveness from both numerical and experimental results and the two approaches were compared.

## 1. Introduction

The understanding of the cavitation erosion phenomenon and the prediction of material damage are a major challenge for hydraulic engineers and scientific researchers. Several experimental and numerical works (as, for example, [1-4]) have been carried out since many years to try to improve the knowledge in this area, but a lot of work remains to be done.

The present article follows up some previous studies developed in our research team these last years, mainly in [5], where cavitating flows on a hydrofoil were investigated from a joint numerical and experimental analysis. A detailed description of the cavity dynamics was carried out and results concerning the cavity length evolution, the shedding frequencies and corresponding Strouhal numbers were presented. In this paper, the focus is given to experimental and numerical evaluations of cavitation aggressiveness.

The considered hydrofoil geometry is described in section 2, as well as the experimental set-up developed. The most original aspects concern unsteady pressure measurements based on a matrix of 8 piezoelectric PVDF sensors (Polyvinylidene Fluoride). Experimental results are described in section 3. Unsteady cavitating flow simulations have been carried out using an in-house two-dimensional (2D) code presented in section 4. From CFD results, the flow aggressiveness has been evaluated by applying the prediction model proposed by Fortes-Patella et al. [6] and synthetized in section 5. Local analyses of unsteady and mean cavitation intensity are also presented and some qualitative comparisons with experimental measurements are illustrated in section 6.

## 2. Hydrofoil geometry and experimental set-up

Figure 1a illustrates the symmetrical hydrofoil geometry considered in the study. Its chord length is c = 100 mm and its maximum thickness is 12 % of the chord length. The hydrofoil has been designed with a large flat area located between 27 % and 70 % of the chord length, which provides room for a matrix of PVDF pressure sensors (figure 1b and table 1). Its rotation axis is at mid chord.

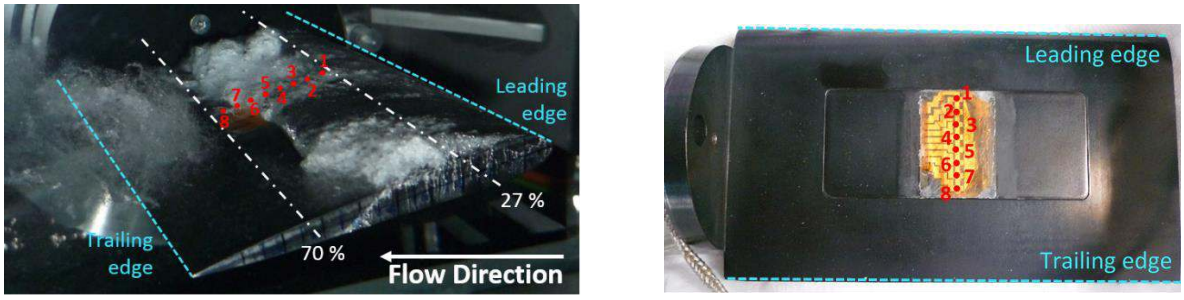


(a) (b)

**Figure 1.** Instrumented hydrofoil (a) under cavitating conditions; (b) top view.

**Table 1.** Positions along the chord of the PVDF pressure sensors.

| Sensor | 1 | 2 | 3 | 4 | 5 | 6 | 7 | 8 |
|---|---|---|---|---|---|---|---|---|
| Position [x/c] | 0.31 | 0.36 | 0.41 | 0.46 | 0.51 | 0.56 | 0.61 | 0.66 |

Experiments have been conducted in the water tunnel of the LEGI laboratory (figure 2). Cavitation number σ is evaluated by:

$$\sigma = \frac{p_{up} - p_v}{\frac{1}{2}\rho V^2}$$

where $p_{up}$ is the upstream pressure, $p_v$ the vapor pressure, ρ the density, and V the test section inlet flow velocity. The uncertainties on V and σ are respectively of 0.01 m/s and 0.02.

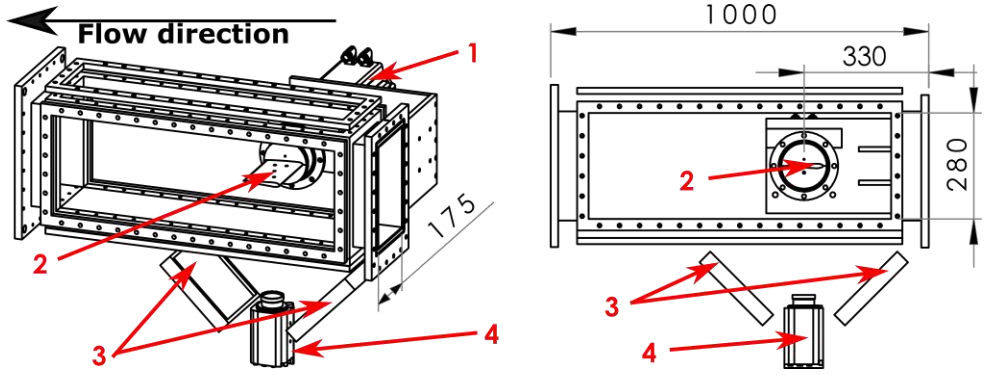


**Figure 2.** Experimental set-up: (1) brushless Kollmorgen motor (AKM74L); (2) hydrofoil; (3) light projectors; (4) high speed camera (MIRO C310). The side of the test section is in Plexiglas. High speed videos have been taken from the bottom at a framerate of 3200 fps.

The unsteady pressure sensors were made from piezoelectric films of thickness $e = 40\ \mu m$. Assuming that both faces are free, the natural frequency of the first mode is $f_N = c/2e$. The lower face, although glued on the metallic hydrofoil, can be considered as free because the insulation and adhesive

layers are relatively thick and have an acoustic impedance very similar to PVDF [7]. Since the speed of sound in the film is $c \cong 2200\, m/s$, the natural frequency is about 27.5 MHz. Such a high natural frequency ensures a rapid response and makes PVDF pressure sensors particularly suitable for the measurement of short duration pressure pulses due to bubble collapses.

A line of 8 square pressure sensors, each of size 2 mm x 2 mm, was fabricated from a metallized PVDF film by the conventional technique of chemical etching. The upper and lower surfaces were protected and electrically insulated by means of a Kapton layer of 60 µm in thickness. When bonded on the hydrofoil, the final sensors had a total thickness of about 200 µm.

Each sensor in final form (including connecting cables) was dynamically calibrated by the ball-dropping method [8]. Pressure sensors were calibrated in load unit (N) and not in pressure (MPa) since their sensitive surface is generally much larger than the size of impact loads due to cavitation bubble collapses so that loading is far from being uniform over the whole sensitive surface. The measured sensitivity slightly changes from one transducer to another and is on the order of 20 mV/N. Pressure sensors were calibrated before and after measurements in the cavitation tunnel in order to detect any possible drift in sensitivity due to sensor ageing or damage by cavitation. The maximum observed decrease in sensitivity is about 20%. It affects primarily the most heavily loaded sensors. The ball-dropping method also allows estimating the mutual interference between neighboring sensors, which was smaller than 5% in terms of the ratio of signal amplitudes.

A series of experimental measurements have been made for velocities of 6, 8 and 10 m/s, upstream cavitation numbers decreasing from 2.2 to 0.3 and for several angles of attack. This paper presents results corresponding to the angle of attack of 4 deg., and for velocities of 8 to 10.4 m/s.

## 3. Experimental results and analyses

Figure 3 illustrates an example of the experimental post-treatment based on high speed video. Each video corresponds to 8300 frames and 2.5 s duration (~110 sheddings). The mean gray profile along the chord is estimated by the spatial averaging over the hydrofoil span (figure 3b). It is calculated for every frame and provides the space-time diagram of the mean gray level shown in figure 3c. From this kind of analyses, one can estimate the maximum cavity length and the shedding frequency for different cavitating conditions [5].

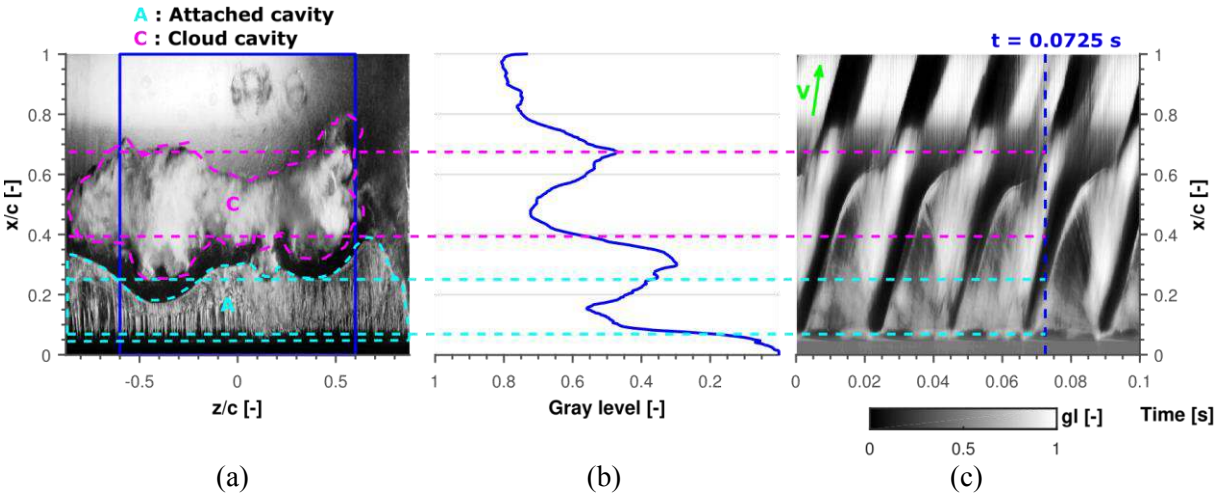


**Figure 3.** (a) Snapshot at t = 0.0725 s. (b) Mean gray profile in the reduced snapshot at t=0.0725 s. (c) Space-time diagram of gray level; black and white are respectively a gray level of 0 and 1. (Angle of attack: 4 deg., V = 8 m/s and σ = 1.1).

An example of unsteady pressure signals obtained by PVDF sensors exposed to cavitating flows is illustrated in figure 4. The sampling frequency is 10 MHz. Experimental signals have been post-treated

by using the MATLAB™ function "findpeaks". The function gives the amplitude, position and duration at mid height of every peak above 1N. This threshold is chosen just above the overall noise. From these measurements, one can analyze the time distribution of the peaks on every pressure sensor, as indicated in figure 5. This figure shows that there is far less than one pulse per shedding cycle for the relatively high threshold of 1 N chosen in this work.

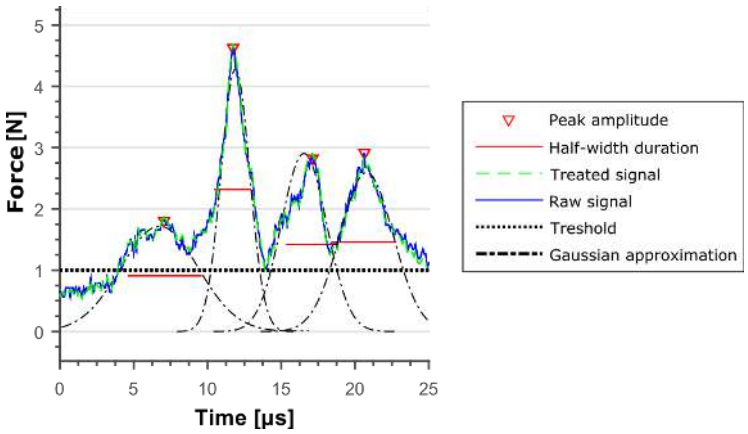


**Figure 4.** Peak detection by the MATLAB™ function "findpeaks".

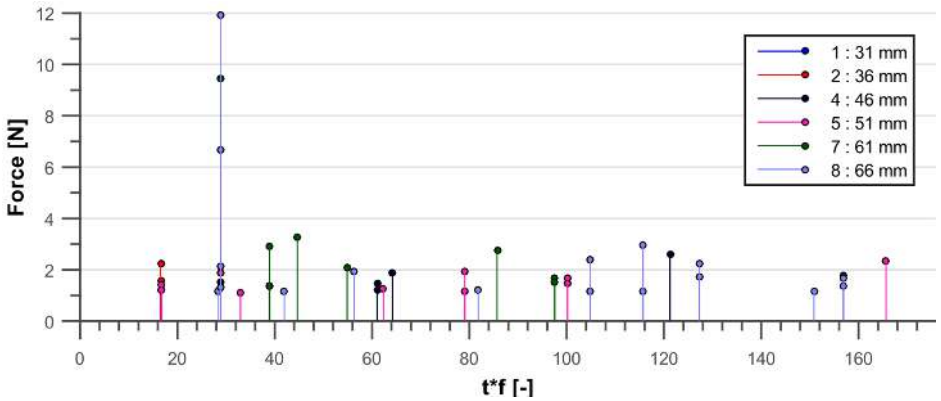


**Figure 5.** Time distribution of the peaks at each pressure transducer. In horizontal axis, the time scale "t" is multiplied by the shedding frequency "f" so that the horizontal axis represents the number of shedding cycles. Results correspond to about 200 vapour shedding cycles.

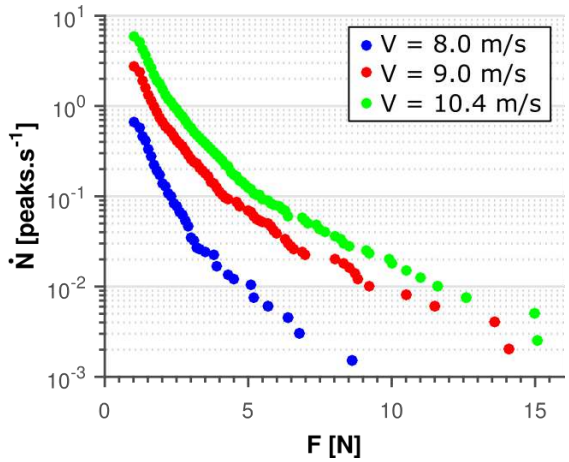


**Figure 6.** Cumulative peak rate as a function of the force on sensor n° 5 for three flow velocities "V" (σ=1.1 and angle of attack: 4 deg.).

Figure 6 illustrates the cumulative peak rate obtained for three different flow velocities at the pressure sensor n° 5. Figure 6 shows that the peak rate significantly increases with flow velocity and that the maximum measured amplitude also increases with flow velocity. These results suggest that the increase in flow aggressiveness is due to an increase in both amplitude and frequency of impact loads.

The same kind of analyses has been done on every sensor: the number of peaks above the threshold F≥1 N has been estimated, divided by the test duration, and the obtained peak frequency has been plotted as a function of the distance to the leading edge for the considered operating points. Figure 7 shows that the maximum aggressiveness is observed in the closure region of the cavity. In the present case, the erosive potential is mostly due to small scale vapor structures that are shed by the leading edge cavity. The large scale cloud that is regularly shed by the cavity generally collapses further downstream (see section 5.2).

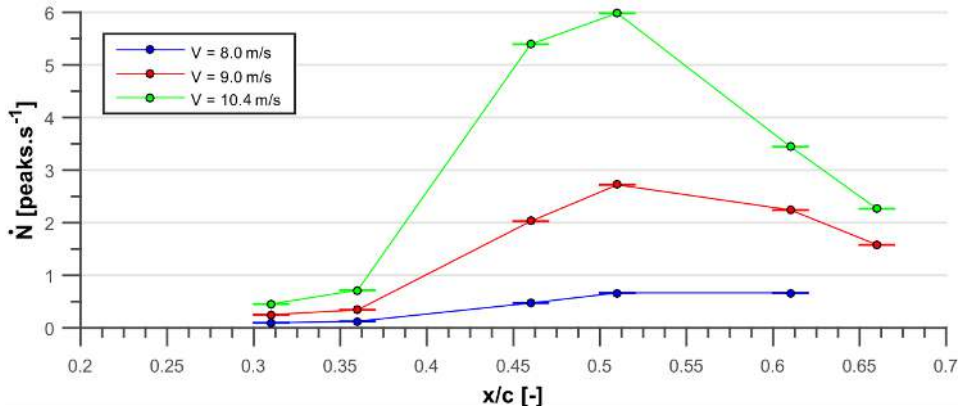


**Figure 7.** Peak rate distribution along the hydrofoil chord for three flow velocities "V". Results have been evaluated from cumulative peak rate histograms corresponding to every sensor by considering a threshold of F ≥ 1 N. (σ =1.1; angle of attack: 4 deg.).

## 4. CFD simulations

Cavitating unsteady flows have been simulated with the in-house 2D code referred to as "IZ". The code is widely described in [9] and was applied and validated in previous studies (for example [6, 10, 12]) in different geometries of hydrofoils, venturis and cascades of hydrofoils. In this numerical tool, Unsteady Reynolds Averaged Navier-Stokes equations are solved for a homogeneous fluid characterized by the mixture density $\rho_m$ defined as a function of the void ratio $\alpha$:

$$\rho_m = \alpha\ \rho_v + (1-\alpha)\rho_l$$

where $\rho_v$ and $\rho_l$ are the vapor and liquid densities, respectively. Pure phases are considered incompressible.

Calculations, in cold water, do not take into account thermodynamic effects and the energy equation is not solved. Two phases are considered to be in dynamic equilibrium in each cell (no drift velocity). The modified k-ε RNG turbulence model developed in LEGI laboratory and detailed in [10] is applied coupled with standard wall functions.

To model the cavitation phenomenon and to close the governing equation system, a barotropic state law is used [9]. The fluid density (and thus the void fraction) is controlled by a ρ(p) law that explicitly links the mixture fluid density to the local static pressure. This law is mainly controlled by its maximum slope, which is related to the minimum speed of sound $c_{min}$ in the mixture. In the present study, $c_{min}$ = 1 m/s, which proved to give good numerical predictions for cold water [10].

The computational H-grids used in the present study is illustrated in figure 8. The dimensionless wall distance y+ of the boundary layer varies between about 20 and 50 under non-cavitating conditions. Usual incompressible boundary conditions are applied: flow velocity is imposed at inlet, and the pressure

(consequently, the downstream cavitation number) is fixed at outlet. The upstream cavitation number fluctuates during unsteady calculations and a numerical mean value of σ is estimated from simulations to carry out comparisons with experiments.

Several calculations were performed in previous work [5] considering different flow conditions. Detailed physical analyses concerning cavity dynamics were presented and the cavitating flow simulations were validated by comparisons with experimental data obtained mainly from high speed videos. Figure 9 presents some results corresponding to the operating point (σ =1.1, V=8m/s and angle of attack: 4 deg.). The behavior of the partial cavity is globally well predicted by the simulations. Shedding frequencies and cavity extensions obtained experimentally and numerically are very similar.

In the present paper, the unsteady CFD results have been used to evaluate the cavitation aggressiveness by applying the prediction model proposed by [6] and described in the next section.

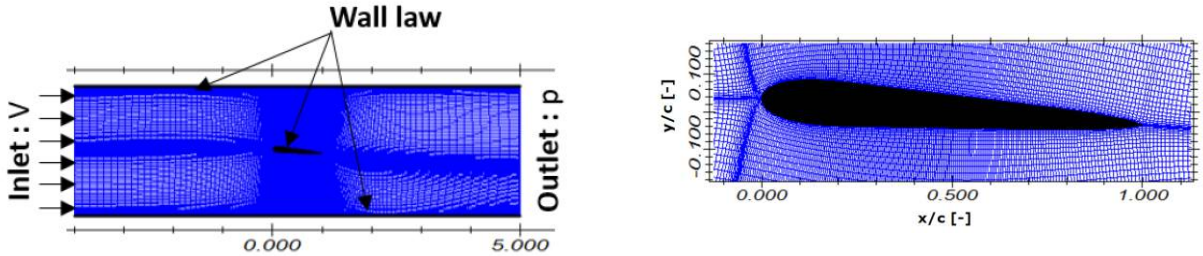


**Figure 8.** Computational domain: applied mesh (320 x 159 nodes) and boundary conditions.

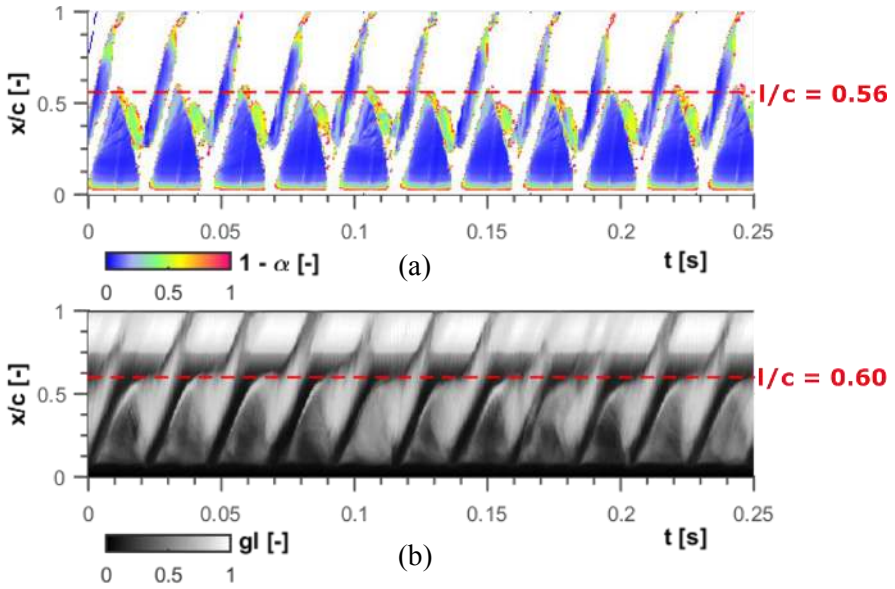


**Figure 9.** Comparisons between numerical (a) and experimental (b) space-time diagrams. *l/c* corresponds to the maximum cavity length observed. In (a), blue and white are respectively for pure vapour and liquid. The void fraction α shown at each point (x, t) is the minimum value of the void fraction along the line x=constant perpendicular to the foil in the (x, y) domain. In (b), *gl* corresponds to "gray level". Numerical shedding frequency *f = 43 Hz*; experimental shedding frequency *f = 48 Hz.* (σ =1.1, V=8m/s and angle of attack: 4 deg.).

## 5. Flow aggressiveness

### *5.1. Prediction model*

The prediction model applied in this article is based on the energy balance approach presented in [6] and was described, tested and qualitatively validated in previous works concerning two other hydrofoils [6, 12, 13]. Based on the idea of Vogel et al. [11], the potential energy of a vapour structure is defined as the vapour volume $V_{vap}$, multiplied by a pressure imbalance:

$$E_{pot} = \Delta P \, V_{vap} \tag{1}$$

where $\Delta P=(P_\infty-P_{vap})$, $P_\infty$ is the surrounding pressure and $P_{vap}$ is the vapour pressure. From this assumption, a volumetric cavitation power $P_{3d}$ can be deduced by computing the Lagrangian derivative of the potential energy to take into account the fact that bubbles are moving with the fluid. The instantaneous volumetric cavitation power is defined by:

$$P_{3d} = \Delta P \frac{DV_{vap}}{Dt} = \Delta P \frac{D\alpha}{Dt} \tag{2}$$

and by using the mass conservation equation:

$$P_{3d} = -\Delta P \frac{\rho}{\rho_l - \rho_v} \mathrm{div}(\vec{U}) \tag{3}$$

for divU < 0 (only the collapse phases are taken into account in the aggressiveness evaluation).

The material is exposed to the collapses of neighbouring vapour structures. To characterize the instantaneous cavitation intensity along the hydrofoil chord, an areal density is evaluated by integrating equation (3):

$$P_{2d} = \int_0^h P_{3d} \, . \, dy \tag{4}$$

where ***h*** is the distance to the solid wall below which it is estimated that the structures are close enough to the wall to be aggressive. In the present work, the value of the distance ***h*** has been considered large enough to take into account all the vapour structures calculated in the computational domain. The influence of this parameter in the aggressiveness prediction was evaluated in [12, 13].

The temporal mean cavitation intensity $P_{mean}$ has been calculated for each hydrofoil surface element by considering several vapour shedding cycles ($T_a$ is the analyses duration), and numerical results have been compared to experimental ones (see section 6).

$$P_{mean} = \frac{1}{T_a} \int_0^{T_a} P_{2d} \, . \, dt \tag{5}$$

### *5.2. Analyses of instantaneous aggressiveness*

From numerical calculations, the time distribution of the cavitation intensity along the hydrofoil can be evaluated, as illustrated in figure 10 and 11. These local analyses allow us to identify the potentially erosive cavitation patterns and to predict the most heavily loaded regions of the hydrofoil. According to numerical analyses corresponding to the operating point ($\sigma$=1.1, V=8m/s and angle of attack: 4 deg.), there are three regions where the cavitation intensity is high. The first one (region I in figure 11) is near the leading edge and correspond to the collapse of an attached small cavity observed in figure 10 (at t*f=0.78). In comparison with experimental observations, 2D numerical predictions generally overestimate the flow aggressiveness in this region [12].

The region II (figure 11) is located around the hydrofoil mid-chord, in the cavity closure region, where the cavity intensity and the damage risks are maximum. The aggressiveness in this region is related to the reentrant jet development shown in figure 10 (from t*f=0.47 to t*f=0.78). In the region III (figure 11), near the trailing edge, the flow aggressiveness is related to the collapse of the shed clouds observed between times t*f=0.21 and t*f=0.47 in figure 10.

## 6. Comparisons between experimental and numerical results

Figure 12 presents a comparison between experimental measurements and numerical predictions of the cavitation aggressiveness for a constant cavitation number (close to 1), a constant angle of attack (4 deg.)

and two different velocities 8 m/s and 10.4 m/s. Right scale shows the computed non-dimensional aggressiveness whereas left scale shows the measured peak rate. Both are plotted as a function of the non-dimensional distance from the hydrofoil leading edge. Numerical and experimental sensors have similar areas (2 mm x 2 mm) and locations.

The prediction of the most aggressive region appears to be in good agreement with the experimental measurements. For both cases and for both experimental and numerical results, the most critical zone corresponds to the closure region of the leading edge cavity (region II in figure 11). Moreover, the predicted width of the critical zone is very similar between experimental and numerical results. At this step, however, the experimental and numerical values of the aggressiveness cannot be compared quantitatively since they do not represent values of the same physical quantity.

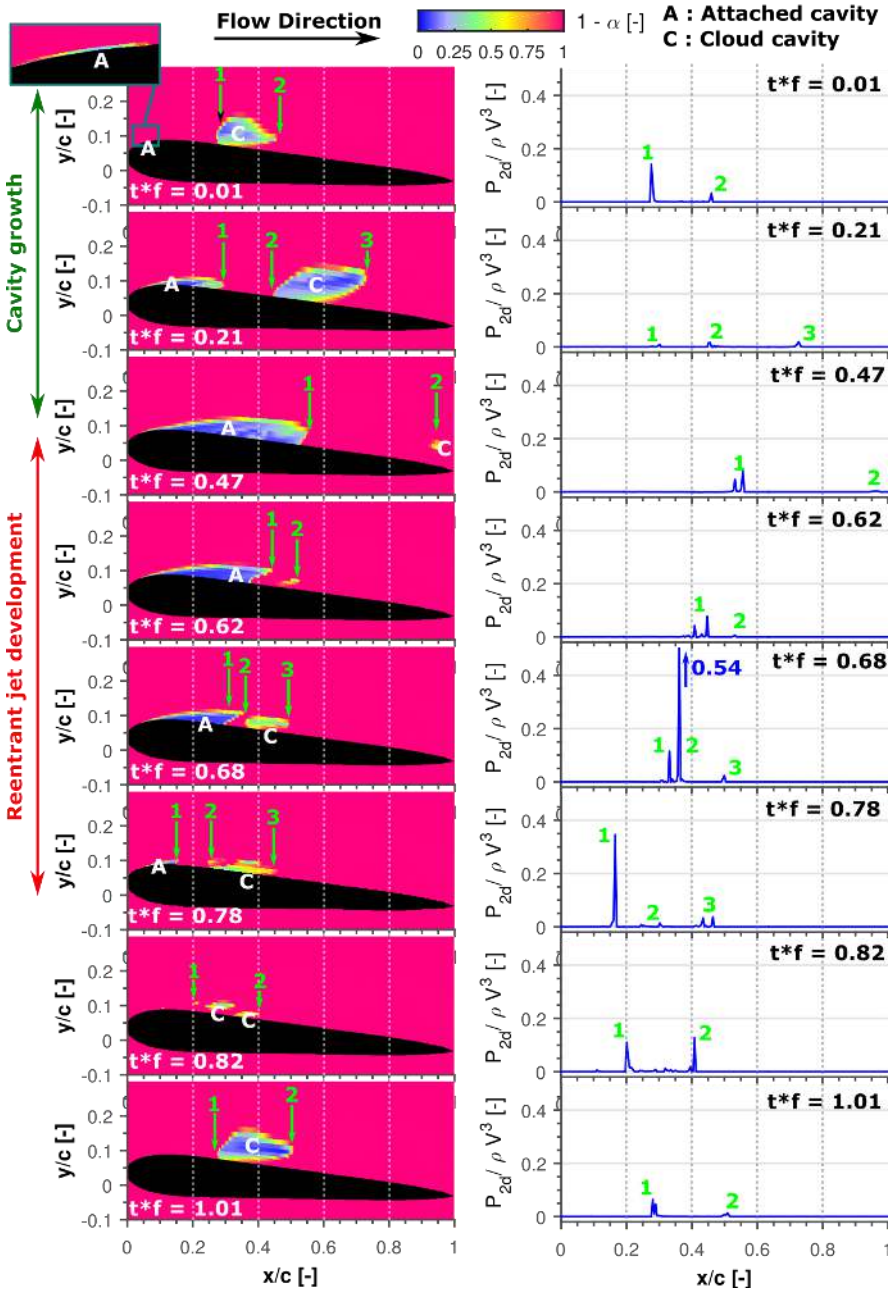


**Figure 10.** Void ratio distribution (at left) and cavitation intensity along the hydrofoil chord (at right) for different time steps during a shedding cycle ($\sigma$ =1.1, V=8m/s and angle of attack: 4 deg.).

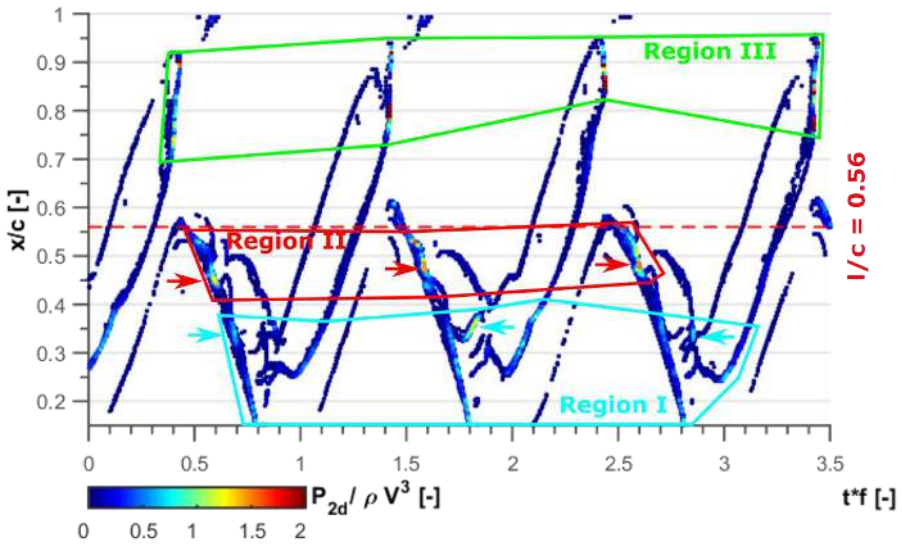


**Figure 11.** Space-time diagram of the cavity intensity corresponding to three shedding cycles. ($\sigma$ =1.1, V=8m/s and angle of attack: 4 deg.).

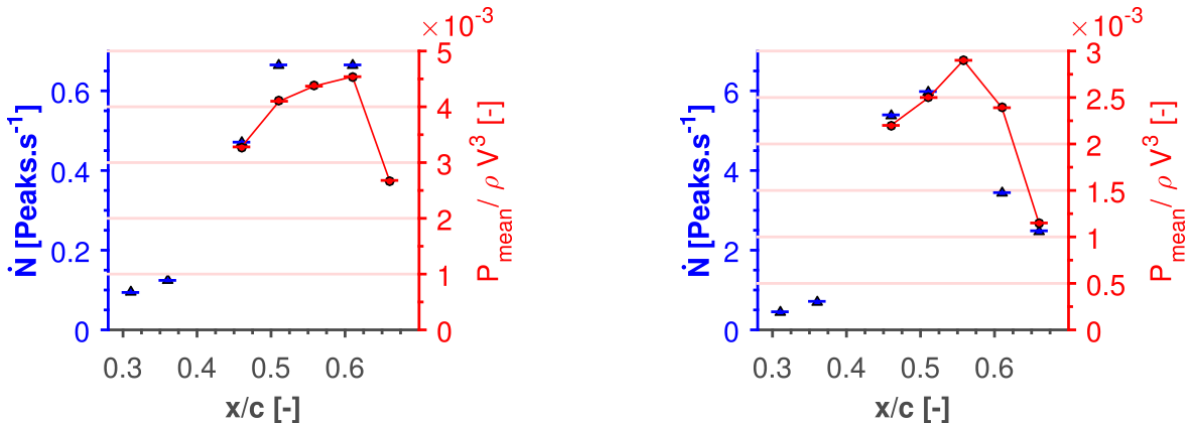


**Figure 12.** Mean values of aggressiveness intensity calculated at the hydrofoil chord – qualitative comparison with experimental results. ($\sigma$~1, angle of attack: 4 deg.). (a) V=8m/s, (b) V=10.4 m/s. Comparative analyses concerns the real aggressive zone observed experimentally on the hydrofoil surface (i.e. x≥0.4c).

## 7. Conclusions

A hydrofoil instrumented with PVDF pressure sensors was tested in the LEGI hydrodynamic tunnel under different cavitating conditions in order to estimate cavitation aggressiveness. The pressure peaks due to the collapse of cavitation structures were measured and compared to flow aggressiveness evaluated by a 2D numerical approach. In spite of 3D effects, the numerical simulations led to a good prediction of the cloud shedding process (including shedding frequency) and of the extension of the aggressive area at cavity closure. Conversely, CFD unsteady results near the leading edge (x<0.4c) disagreed with experimental observations since the aggressiveness predicted in this area is overestimated. 3D approaches (e.g. [13]) are needed to obtain a better simulation in this zone, but remain very time-consuming. In any case, the proposed aggressiveness model, associated with suitable CFD

tools, represents a promising approach to predict and control cavitation erosion damage in real hydraulic systems and machinery.

**Acknowledgements**
The authors gratefully acknowledge the Foundation Grenoble INP through the industrial chair GE (General Electric) "HYDRO'LIKE". The code "IZ" was developed at the LEGI with the support of the CNES (Centre National d'Etudes Spatiales).

**References**

[1] Pereira F, Avellan F and Dupont JM. 1998 Prediction of cavitation erosion: an energy approach *Journal of Fluid Engineering , Transactions of the ASME* **120**
[2] Petkovšek M and Dular M 2013 Simultaneous observation of cavitation structures and cavitation erosion *Wear* **300**
[3] Ochiai N, Iga Y, Nohmi M and Ikohagi T 2010 Numerical prediction of cavitation erosion intensity in cavitating flows around a clark y 11.7% hydrofoil *Journal of Fluid Science and Technology* **5**
[4] Schmidt S, Mihatsch M, Thalhamer M and Adams N 2014 Assessment of erosion sensitive areas via compressible simulation of unsteady cavitating flows *Advanced experimental and numerical techniques for cavitation erosion prediction*, pp. 329-344
[5] Carrat JB, Fortes-Patella R and Franc JP 2017 Assessment of cavitating flow aggressiveness on a hydrofoil: experimental and numerical approaches *ASME 2017 Fluids Engineering Division Summer Meeting* Paper No. FEDSM2017-69187, pp. V01AT05A013
[6] Fortes-Patella R, Archer A and Flageul C 2012 Numerical and experimental investigations on cavitation erosion. *IOP Conference Series : Earth and Environmental Science* **15**(2):022013
[7] Brown LF 2000 Design considerations for piezoelectric polymer ultrasound transducers *IEEE Transactions on Ultrasonics, Ferroelectrics and Frequency Control* **47**(6): p. 1377-1396
[8] Soyama H, Lichtarowicz A, Momma T and Williams EJ 1998 A new calibration method for dynamically loaded transducers and its application to cavitation impact measurement *Journal of Fluids Engineering, Transactions of the ASME* **120**(4): p. 712-718
[9] Coutier-Delgosha O, Reboud JL and Delannoy Y 2003 Numerical simulation of the unsteady behaviour of cavitating flows *Int. J. for Numerical Meth. in Fluids* **42**, pp. 527-548
[10] Coutier-Delgosha O, Fortes-Patella R and Reboud JL 2003 Evaluation of the turbulence model influence on the numerical simulations of unsteady cavitation *Journal of Fluids Engineering*, *Transactions of the ASME* **125** pp. 38-45
[11] Vogel A, Lauterborn W and Timm R 1989 Optical and acoustic investigations of the dynamics of laser-produced cavitation bubbles near a solid boundary *Journal of Fluid Mechanics* **206**, pp. 299-338
[12] Flageul C, Fortes Patella R and Archer A 2012 Cavitation erosion prediction by numerical cavitation *Proc. of 14th International Symposium on Transport Phenomena and Dynamics of Rotating Machinery ISROMAC-14*, Honolulu, HI, USA
[13] Leclercq C, Archer A and Fortes-Patella R 2016 Numerical investigations on cavitation intensity for 3d homogeneous unsteady viscous flows *IOP Conference Series: Earth and Environmental Science* http://iopscience.iop.org/1755-1315/49/9/092007